

SELF-SIMILAR SOLUTIONS FOR THE TRIPLE POINT PARADOX IN GASDYNAMICS*

ALLEN M. TESDALL[†], RICHARD SANDERS[‡], AND BARBARA L. KEYFITZ[†]

Abstract. We present numerical solutions of a two-dimensional Riemann problem for the compressible Euler equations that describes the Mach reflection of weak shock waves. High resolution finite volume schemes are used to solve the equations formulated in self-similar variables. We use extreme local grid refinement to resolve the solution in the neighborhood of an apparent but mathematically inadmissible shock triple point. The solutions contain a complex structure: instead of three shocks meeting in a single standard triple point, there is a sequence of triple points and tiny supersonic patches behind the leading triple point, formed by the reflection of weak shocks and expansion waves between the sonic line and the Mach shock. An expansion fan originates at each triple point, resolving the von Neumann triple point paradox.

Key words. triple point paradox, von Neumann paradox, self-similar solutions

AMS subject classifications. 65M06, 35L65, 76L05

DOI. 10.1137/070698567

1. Introduction. Consider a plane normal shock in an inviscid, compressible, perfect gas which hits a fixed wedge with half angle θ_w , as depicted in Figure 1. For a given upstream state with density $\rho = \rho_r$, velocity $\mathbf{u} = (u, v) = (0, 0)$, and pressure $p = p_r$, the fluid properties downstream of a *fast* (i.e., $u + c$) shock are given by

$$(1.1) \quad \begin{aligned} \frac{\rho_l}{\rho_r} &= \frac{(\gamma + 1) M^2}{2 + (\gamma - 1) M^2}, & \frac{u_l}{c_r} &= \frac{2}{\gamma + 1} \left(M - \frac{1}{M} \right), \\ \frac{p_l}{p_r} &= \frac{2\gamma}{\gamma + 1} M^2 - \frac{\gamma - 1}{\gamma + 1}, \end{aligned}$$

where γ is the ratio of specific heats and $M > 1$ is the shock Mach number, defined as the shock speed given by the Rankine–Hugoniot relations divided by the upstream sound speed $c_r = \sqrt{\gamma p_r / \rho_r}$. Following interaction of the shock with the wedge wall, a number of self-similar reflection patterns are possible, depending on the values of M and θ_w . The simplest pattern is *regular reflection*, in which there is a single reflected shock, depicted in Figure 1(a). For small wedge angles or strong shocks, regular reflection is replaced by *Mach reflection*. The simplest type of Mach reflection is called single Mach reflection, in which the incident and reflected shocks move off the wedge and a single shock called the Mach stem extends down to the wall; see Figure 1(b). The point where the three shocks meet is called the triple point, and a contact discontinuity also originates there.

*Received by the editors July 30, 2007; accepted for publication (in revised form) January 2, 2008; published electronically DATE.

<http://www.siam.org/journals/siap/x-x/69856.html>

[†]Fields Institute, Toronto, ON M5T 3J1, Canada, and Department of Mathematics, University of Houston, Houston, TX 77204 (atesdall@fields.utoronto.ca, bkeyfitz@fields.utoronto.ca). The first author’s research was supported by National Science Foundation grant DMS 03-06307, NSERC grant 312587-05, and the Fields Institute. The third author’s research was supported by National Science Foundation grant DMS 03-06307, Department of Energy grant DE-FG02-03ER25575, and NSERC grant 312587-05.

[‡]Department of Mathematics, University of Houston, Houston, TX 77204 (sanders@math.uh.edu). This author’s research was supported by National Science Foundation grant DMS 03-06307.

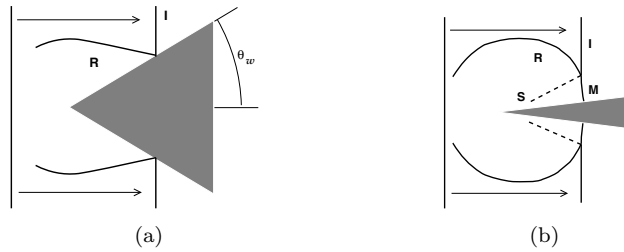


FIG. 1. A planar shock moving from left to right impinges on a wedge. After contact, I indicates the incident shock and R indicates the reflected shock. Regular reflection is depicted in (a) and Mach reflection in (b). In (b), the dotted line S indicates a contact discontinuity and M is the Mach stem.

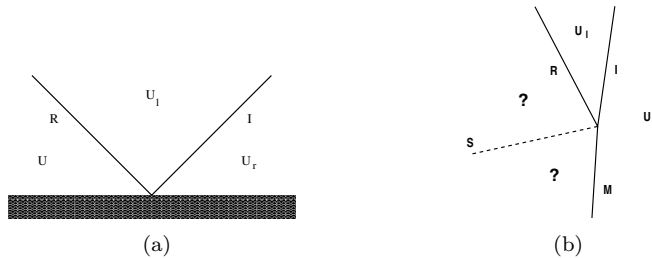


FIG. 2. An enlargement of the incident and reflected shock intersections in Figure 1. Regular reflection is depicted in (a) and Mach reflection in (b). The constant states upstream and downstream of the incident shock are denoted by U_r and U_i . Whether or not constant states indicated by the question marks in (b) exist depends on the strength of I .

The basic equations that describe regular and Mach reflection were formulated by von Neumann in 1943 [10] and are known as two-shock and three-shock theory, respectively. His analysis is based on the assumption that Mach reflection solutions can be locally approximated by constant states separated by plane discontinuities (this is also true, in a finite neighborhood, for flows that are supersonic at the reflection point; see Figure 2 for an illustration of this assumption). The oblique shock relations of gasdynamics connect the constant states. To explain transition between regular and Mach reflection, von Neumann suggested several criteria. For weak incident shocks he proposed that transition occurs at the detachment angle, which is a function of M . For a shock with a given M impinging on a wedge, when the wedge angle is larger than the detachment angle there are two regular reflection solutions, one with a strong reflected shock and one with a weak reflected shock (only the weak reflected shock solution is observed experimentally). At the detachment angle the two solutions coalesce, and for smaller wedge angles there is no regularly reflected solution. This is a possible condition for transition but has not been definitively established. Several criteria for transition can be obtained using von Neumann's approach; see Henderson [7] for a detailed discussion.

Good agreement between the von Neumann theory and experiment is obtained for regular and Mach reflection for a wide range of conditions. For sufficiently weak shocks, however, application of the three-shock theory indicates that triple point solutions such as those depicted in Figure 2(b) do not exist. Transition from regular to Mach reflection is impossible, and the theory is unable to predict what kind of reflection does occur for weak shocks reflecting off thin wedges. However, experiments in which a very weak shock reflects off a thin wedge appear to show a pattern

of reflection containing three shocks meeting at a triple point. This discrepancy is referred to as the von Neumann, or triple point, paradox.

Over the years, a number of ways to resolve the paradox have been proposed. A singularity could occur in the solution behind the triple point [15] or in the reflected shock curvature at the triple point [14], so that a local approximation of the solution by plane waves separated by constant states is invalid; there could be an unobserved fourth shock at the triple point [6]; or the reflected shock could decay into a continuous wave before hitting the incident shock, so that there is no triple point [4]. In 1947 Guderley [5] proposed the existence of an expansion fan and a supersonic region behind the triple point in a steady weak shock Mach reflection (the same triple point paradox occurs in the case of steady flow as in unsteady reflection off a wedge). He demonstrated that one could construct local solutions consisting of three plane shocks, an expansion fan, and a contact discontinuity meeting at a point. However, despite intensive study, no evidence of an expansion fan or a supersonic patch was seen either in experiments (see, for example, [1, 11, 14]) or in numerical solutions (see [4, 2, 15]).

The first indication that Guderley's proposed resolution might be essentially correct was contained in numerical solutions of shock reflection problems for the unsteady transonic small disturbance equations (UTSDE) in [8] and the compressible Euler equations in [18]. Solutions containing a supersonic patch embedded in the subsonic flow directly behind the triple point in a weak shock Mach reflection were presented there. Subsequently, Zakharian et al. [19] found a supersonic region in a numerical solution of the compressible Euler equations. The supersonic region in all of these solutions is extremely small, explaining why it had never been observed before, experimentally or numerically.

The supersonic patches obtained in the solutions in [8, 18, 19] appeared to confirm Guderley's four wave solution. The patch indicates that it is plausible for an expansion fan to be an unobserved part of the observed three-shock confluence, since the flow must be supersonic for an expansion wave to occur. However, these solutions are not sufficiently well resolved to show the structure of the flow inside the supersonic region. In [16] numerical solutions were obtained of a problem for the UTSDE that describes the reflection of weak shocks off thin wedges, with the equations formulated in special self-similar variables. The advantage of using self-similar coordinates is that the point of interest remains fixed on the computational grid, and a steady self-similar solution is obtained by letting a pseudotime $t \rightarrow \infty$. In a parameter range for which regular reflection is impossible, the solutions contain a remarkably complex structure: there is a sequence of triple points and tiny supersonic patches immediately behind the leading triple point, formed by the reflection of weak shocks and expansion fans between the sonic line and the Mach shock. A centered expansion fan originates at each triple point. It was shown that the triple points with expansion fans observed numerically are consistent with theory and resolve the paradox. The term *Guderley Mach reflection* was chosen in [9] to name this new reflection pattern.

Following the detection of Guderley Mach reflection in [16], a problem for the nonlinear wave system that is analogous to the reflection of weak shocks off thin wedges was studied numerically in [17]. The nonlinear wave system is a simple 3×3 hyperbolic system which resembles the Euler equations, but is not obtained from them via a limit, and which has no known physical relevance. It is obtained from the isentropic Euler equations by dropping the momentum transport terms from the momentum equations, and it has a characteristic structure similar to that of the compressible

Euler equations: nonlinear acoustic waves coupled (weakly) with linearly degenerate waves. In a parameter range where regular reflection is not possible, a numerical solution of this system formulated in self-similar variables was obtained which again contains a sequence of triple points in a tiny region behind the leading triple point, with a centered expansion fan originating at each triple point. This solution is very similar in pattern to those obtained for the UTSDE. The discovery of Guderley Mach reflection in a solution of this system leads one to expect that a sequence of supersonic patches and triple points is a generic feature of two-dimensional Riemann problems for some class of hyperbolic conservation laws. This class is possibly characterized by “acoustic waves,” as defined in [3]. The compressible Euler system for gasdynamics is another member of this class, suggesting that weak shock solutions of the Euler equations—the subject of the present work—would contain Guderley Mach reflection solutions as well.

The numerical solutions in [8, 18, 19] were obtained by solving an initial value problem for the unsteady equations. The problem of inviscid shock reflection at a wedge is self-similar, and there are advantages to solving the problem in self-similar, rather than unsteady, variables. In the unsteady formulation local grid refinement near the triple point is difficult, because any waves which are present initially move through the numerical domain, requiring the refined region to move as well. Solutions of the self-similar equations are stationary, making local grid refinement easier to implement. Also, in self-similar variables a global grid continuation procedure can be used in which a partially converged solution on a coarse grid is interpolated onto a fine grid and then driven to convergence on the fine grid. Procedures for solving the UTSDE in self-similar variables were developed in [16] and extended to apply to the nonlinear wave system in [17]. The procedures used to solve the nonlinear wave system have been applied, with only slight modification, in the present work to obtain solutions of the full Euler system.

In this paper we present high resolution numerical solutions of the shock reflection problem for the full Euler equations computed in self-similar coordinates. Our most highly resolved solution shows that Guderley Mach reflection occurs at a set of parameter values where Mach reflection is impossible: there is a sequence of tiny supersonic patches and triple points behind the leading triple point in a weak shock Mach reflection. This numerical solution is remarkably similar to those obtained for the UTSDE in [16] and for the nonlinear wave system in [17].

Experimental confirmation of these results is challenging simply because the computed structure is so small and weak. Nevertheless, recent experimental evidence appears to confirm that Guderley Mach reflection occurs when a weak shock reflects off a thin wedge. Skews and Ashworth in [12] modified an existing shock tube in order to obtain Mach stem lengths more than an order of magnitude larger than those possible with conventional shock tubes. They present photographic images of shock reflection experiments that clearly show an expansion wave behind the triple point in a weak shock Mach reflection, a terminating shocklet, and evidence of a second terminating shocklet. The supersonic region is extremely small, as predicted by the computations in [16, 17] and the present work. Further experimental improvements and data acquisition are underway.

This paper is organized as follows. In section 2 we describe the shock reflection problem for the full Euler equations. In section 3 we discuss our approach to solving this problem numerically. The numerical results obtained are presented in section 4. In section 5 we discuss questions raised by our results. Finally, we summarize our findings in section 6.

2. The shock reflection problem for the Euler equations. We consider a problem for the full Euler equations that describes the reflection of a shock wave off a wedge. The shock reflection problem consists of the compressible Euler equations,

$$(2.1) \quad \begin{aligned} \rho_t + (\rho u)_x + (\rho v)_y &= 0, \\ (\rho u)_t + (\rho u^2 + p)_x + (\rho uv)_y &= 0, \\ (\rho v)_t + (\rho uv)_x + (\rho v^2 + p)_y &= 0, \\ (\rho e)_t + ((\rho e + p)u)_x + ((\rho e + p)v)_y &= 0, \end{aligned}$$

with piecewise constant Riemann data consisting of two states separated by a discontinuity located at $x = 0$. Here, ρ is the density, u and v are the x and y components of velocity, respectively, p is the pressure, and e is the energy. We use an ideal gas equation of state,

$$p = (\gamma - 1)\rho \left(e - \frac{1}{2}(u^2 + v^2) \right),$$

where the ratio of specific heats γ is taken to be 1.4. The initial data correspond to a vertical plane shock hitting the corner of a wedge at $t = 0$. Letting $U(x, y, t) = (\rho, u, v, p)$,

$$(2.2) \quad U(x, y, 0) = \begin{cases} U_R \equiv (\rho_R, 0, 0, p_R) & \text{if } x > 0, \\ U_L \equiv (\rho_L, u_L, 0, p_L) & \text{if } x < 0, \end{cases}$$

where the left- and right-hand states are connected by the Rankine–Hugoniot jump conditions for a shock with Mach number M . The boundary condition on the wedge wall is

$$(2.3) \quad \mathbf{u} \cdot \mathbf{n} = 0,$$

where $\mathbf{u} = (u, v)$ and \mathbf{n} is the unit normal vector at the wall. The shock propagates to the right into stationary gas with speed Mc , where c is the sound speed in the fluid ahead of the shock at state U_R . The location of the incident shock is given by

$$(2.4) \quad x = (Mc)t.$$

For a gas with a given equation of state, there are two parameters in the shock reflection problem: the wedge angle θ and the strength of the incident shock, which we parameterize by the shock Mach number M . For sufficiently small Mach numbers and small wedge angles, neither Mach reflection nor regular reflection solutions exist (see [7, 10]).

3. The numerical method. The problem (2.1)–(2.3) is self-similar, so the solution depends only on the similarity variables

$$\xi = \frac{x}{t}, \quad \eta = \frac{y}{t}.$$

We write (2.1) in the form

$$(3.1) \quad U_t + F_x + G_y = 0,$$

where

$$\begin{aligned} U &= (\rho, \rho u, \rho v, \rho e), \quad F = (\rho u, \rho u^2 + p, \rho uv, \rho ue + up), \\ \text{and } G &= (\rho v, \rho uv, \rho v^2 + p, \rho ve + vp). \end{aligned}$$

Writing (3.1) in terms of ξ , η , and a pseudotime variable $\tau = \log t$, we obtain

$$(3.2) \quad U_\tau - \xi U_\xi - \eta U_\eta + F_\xi + G_\eta = 0.$$

As $\tau \rightarrow +\infty$, solutions of (3.2) converge to a pseudosteady, self-similar solution that satisfies

$$(3.3) \quad -\xi U_\xi - \eta U_\eta + F_\xi + G_\eta = 0.$$

Equation (3.3) is hyperbolic when $c^2 < \bar{u}^2 + \bar{v}^2$, corresponding to supersonic flow in a self-similar coordinate frame, and of mixed type when $c^2 > \bar{u}^2 + \bar{v}^2$, corresponding to subsonic flow, where $\bar{u} = u - \xi$, $\bar{v} = v - \eta$. Here, $c = \sqrt{\gamma p / \rho}$ is the local sound speed. The sonic line is given by

$$(3.4) \quad \bar{u}^2 + \bar{v}^2 = c^2.$$

By abuse of notation, we have referred to the locus of transition points between $c^2 < \bar{u}^2 + \bar{v}^2$ and $c^2 > \bar{u}^2 + \bar{v}^2$ as the sonic line, whether the flow is continuous there or not. We define a local self-similar Mach number $\bar{M}^2 = \frac{\bar{u}^2 + \bar{v}^2}{c^2}$. When $\bar{M} > 1$, the flow is supersonic, and when $\bar{M} < 1$, the flow is subsonic.

In order to solve (3.2) numerically, we write it in conservative form as

$$(3.5) \quad U_\tau + (F - \xi U)_\xi + (G - \eta U)_\eta + 2U = 0.$$

In these self-similar variables, the full Euler system has the form of the unsteady equations (3.1) with modified flux functions and a lower-order source term.

An essential feature of our numerical method is the use of local grid refinement in the area of the apparent triple point. We designed a sequence of successively refined, nonuniform, logically rectangular finite volume grids. See Figure 3 for a diagram of the computational domain. We use grid continuation, in which partially converged coarse grid solutions are interpolated onto more refined grids and converged on the refined grids. For each grid, inside a given box surrounding the triple point, uniform grid spacing is used. Outside of this box, the grid is exponentially stretched in both grid directions.

The basic finite volume scheme is quite standard. Each grid cell, Ω , is a quadrilateral, and using $\vec{\nu} = (\nu_\xi, \nu_\eta)$ to denote the normal vector to a typical side of Ω , numerical fluxes are designed to be consistent with

$$\tilde{F}(U) = (F(U) - \xi U) \nu_\xi + (G(U) - \eta U) \nu_\eta = \begin{pmatrix} \nu_\xi \rho u + \nu_\eta \rho v - \bar{\xi} \rho \\ \nu_\xi (\rho u^2 + p) + \nu_\eta \rho u v - \bar{\xi} \rho u \\ \nu_\xi \rho u v + \nu_\eta (\rho v^2 + p) - \bar{\xi} \rho v \\ \nu_\xi (\rho u e + u p) + \nu_\eta (\rho v e + v p) - \bar{\xi} \rho e \end{pmatrix},$$

where $\bar{\xi} = (\vec{\xi} \cdot \vec{\nu})$ and $\vec{\xi} = (\xi, \eta)$. Since $\vec{\xi}$ varies, our numerical flux formulae evaluate $\vec{\xi}$ frozen at the midpoint of each cell side. We use essentially the same numerical scheme as in [17], a high-order scheme based on the Roe numerical flux. High-order accuracy is achieved by using piecewise quadratic reconstruction limited in characteristic variables, together with the Roe flux

$$H_{Roe} = \frac{1}{2} (\tilde{F}(U_l) + \tilde{F}(U_r) - R \Lambda L (U_r - U_l)),$$

where $\Lambda = \text{diag}(|-\bar{\xi} - c|, |-\bar{\xi}|, |-\bar{\xi} + c|)$, and R and L are the matrices of right and left eigenvectors to the Jacobian of \tilde{F} . As in [17], we simplify the Roe approach by

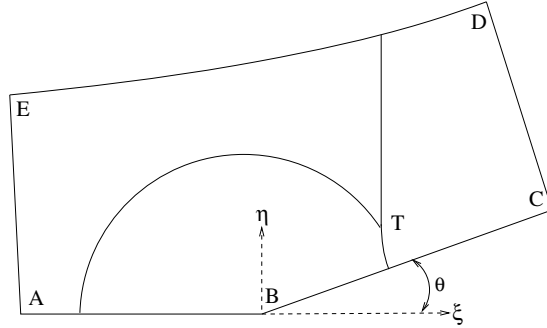


FIG. 3. A schematic diagram of the computational domain. ABC is the wall; BC is the wedge, with angle θ . $CDEA$ is the far field numerical boundary. The incident shock is perpendicular to AB . The incident (above T), reflected (left of T), and Mach (below T) shocks meet at the triple point T .

evaluating R and L at the midpoint $U_{Roe} = \frac{1}{2}(U_l + U_r)$, which for the Euler equations is only an approximation to the Roe average. To avoid spurious expansion shocks, artificial dissipation on the order of $|U_r - U_l|$ is appended to the diagonal part of the Roe dissipation matrix in a field-by-field manner.

Time integration is accomplished using Heun's method, which can be written in two step predictor-corrector form (using overbars to denote predicted values) as

$$\begin{aligned} \frac{U^{\overline{n+1}} - U^n}{\Delta\tau} + \frac{1}{|\Omega|} \int_{\partial\Omega} H_{Roe}^n ds + 2U^n &= 0, \\ \frac{2U^{n+1} - U^{\overline{n+1}} - U^n}{\Delta\tau} + \frac{1}{|\Omega|} \int_{\partial\Omega} H_{Roe}^{\overline{n+1}} ds + 2U^{\overline{n+1}} &= 0. \end{aligned}$$

3.1. The grid and boundary conditions. We computed solutions of the problem (2.1)–(2.3) in the finite computational domain shown schematically in Figure 3. We use a nonuniform grid with a locally refined area of uniformly spaced grid very close to the triple point, as illustrated in Figure 4. The grid is defined by a conformal map of the form $z = w^\alpha$, so it is orthogonal with a singularity at the ramp apex $x = y = 0$. The refined uniform grid area is so small that it is obscured in the main plot shown in Figure 4. The inset plots show enlargements of the grid in the indicated rectangular regions, and the smaller inset plot contains a small superimposed box which delineates the refined uniform grid region. The grid is stretched exponentially from the edge of the uniform grid region to the outer numerical boundaries and the wall, with a stretching factor of 1%.

We use a sequence of such grids, with each grid corresponding to a level of grid refinement. The uniform grid region of each grid is refined by a factor of two in both x/t and y/t in relation to the uniform grid region of the previous grid. We obtain solutions on coarse grids, interpolate these onto more refined grids, and converge the solutions on the refined grids. We repeat this process until no further change is observed in the solution near the apparent triple point and *grid continue* to a steady state. This process is illustrated in Figure 5, which shows a coarse grid (dashed lines) overlaid with a refined grid (solid lines) in the uniform grid region of both grids. A solution is obtained on the coarse grid, and the computation on the coarse grid is stopped. This solution is interpolated onto the refined grid, and the computation

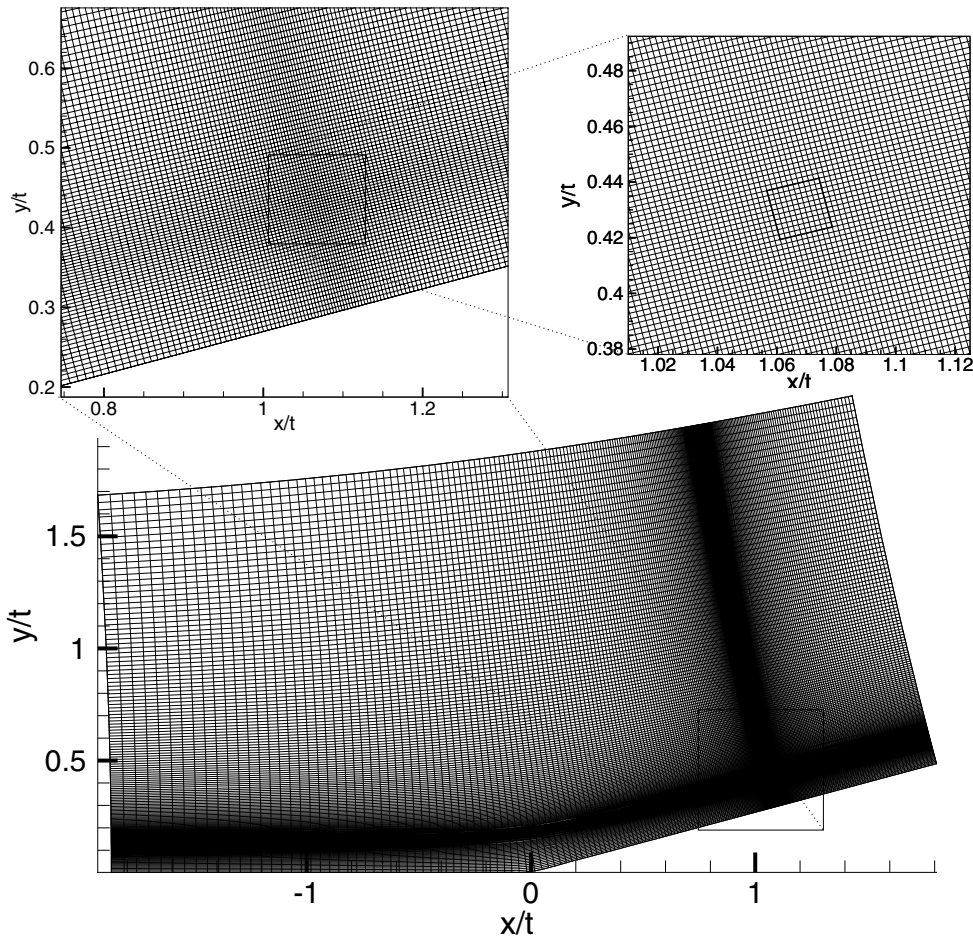


FIG. 4. The grid structure, illustrating the region of uniform local refinement, which is outlined by the small box superimposed on the grid in the inset plot at the upper right. Outside of this small box, the grid is stretched. The main plot shows the entire grid. The locally refined region in this very coarse grid contains 10×10 grid cells, with $\Delta\xi = \Delta\eta = 0.002$. The locally refined region in our most refined grid is shown in Figure 7(a).

is resumed on the refined grid. We found that bilinear interpolation gave the best results, while higher-order methods such as biquadratic interpolation resulted in large overshoots at the shocks.

Every grid in the sequence is designed so that the refined uniform grid region surrounds the apparent triple point as it appears in the currently available solution (the solution obtained with the previous grid). As the grids are refined and the shocks become better resolved, the triple point location can be determined more precisely, and the refined grid area can be repositioned and reduced in size. In fact, the refined uniform grid region depicted in the coarse grid shown in Figure 4 is more than 1000 times as large as the refined uniform grid region in our finest grid. The total number of grid cells in our finest grid is approximately six million, of which $300 \times 1000 = 3 \times 10^5$ ($\Delta\xi = \Delta\eta = 1 \times 10^{-6}$) are devoted to the local refinement.

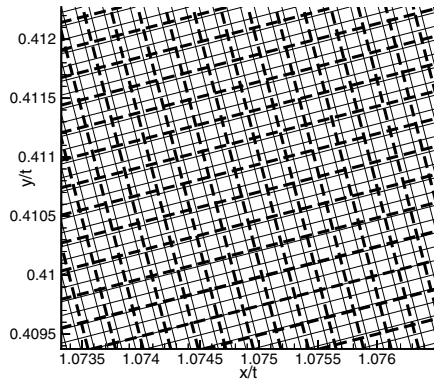


FIG. 5. A solution on a coarse grid such as the one depicted in Figure 4 is interpolated onto a refined grid and converged on the refined grid. The locally refined region of the coarse grid (dashed lines) in this example has $\Delta\xi = \Delta\eta = 0.00025$, and the fine grid (solid lines) has $\Delta\xi = \Delta\eta = 0.000125$. The region shown in the plot is in the locally refined region of both grids.

On the wall boundary ABC in Figure 3 we impose reflecting boundary conditions, equivalent to the physical no-flow condition (2.3). In addition, we require numerical boundary conditions on the outer computational boundaries, which we determine as follows.

The incident shock location (2.4) in self-similar variables is

$$\xi = Mc,$$

where c is the sound speed ahead of the shock. Boundary data on the left, right, and top are given to exactly agree with this shock, so that

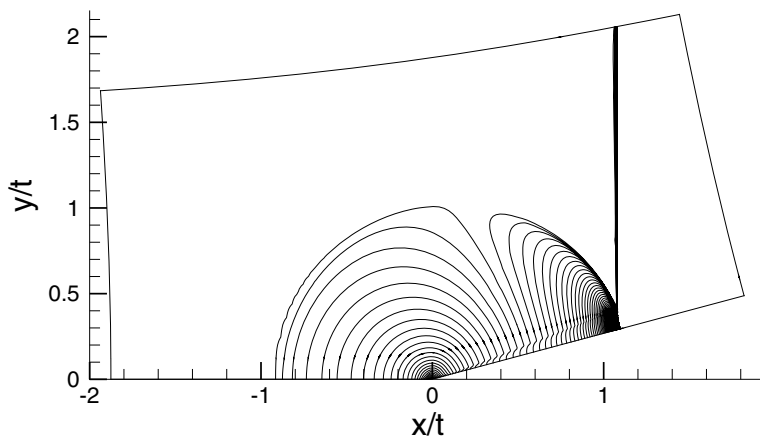
$$(3.6) \quad U(\xi, \eta) = \begin{cases} U_R, & \xi > Mc, \\ U_L, & \xi < Mc, \end{cases}$$

where the fluid properties U_L behind the shock are obtained from the Rankine–Hugoniot conditions. We use (3.6) as a boundary condition for (3.5) on $CDEA$.

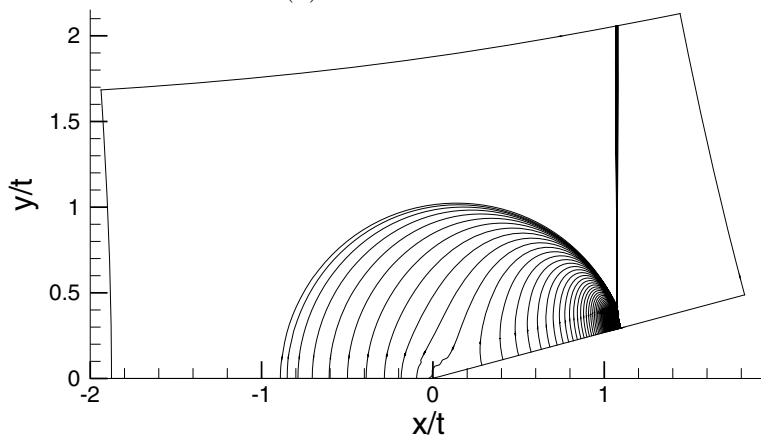
4. Numerical results. We computed numerical solutions of (2.1)–(2.3) for a shock Mach number M equal to 1.075 and a wedge angle θ equal to 15 degrees. These data correspond to parameter $a \approx 1/2$ in the UTSDE model used in [16]. This problem is well outside the range for which regular reflection can occur. However, Mach reflection is also not possible for shocks this weak, and so this example illustrates a classic triple point paradox. In our computations we used $\rho_R = 1.4$ and $p_R = 1$ in (2.2) and determined the values U_L behind the shock from the Rankine–Hugoniot conditions. Table 4.1 gives the initial values of the fluid variables. We give our finest grid results in the plots which follow. Figure 6(a)–(b) shows a numerical solution that gives an overall picture of the shock reflection. The plots in (a) and (b) show Mach number and pressure contours, respectively, as functions of $(x/t, y/t)$. Here, we refer to the local Mach number of the solution, not to the shock Mach number M . The numerical solution appears to show a simple Mach reflection, with three shocks meeting at a triple point. Ahead of the incident shock, the pressure is equal to 1 and

TABLE 4.1
 Left and right states for an incident shock with Mach number $M = 1.075$ and $\gamma = 1.4$.

	ρ	u	v	p
Right	1.4	0	0	1
Left	1.57697	0.12064	0	1.18156



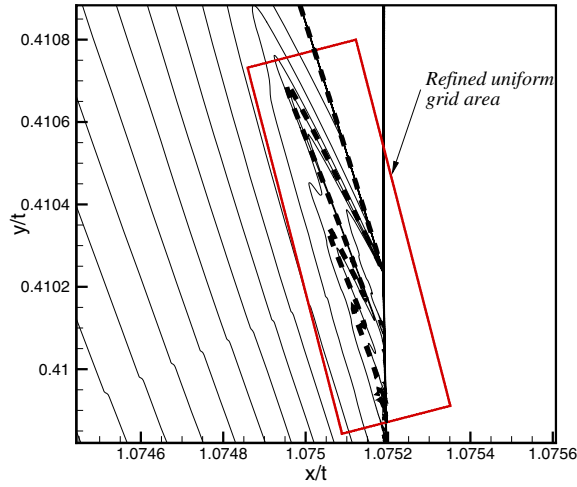
(a) Mach number



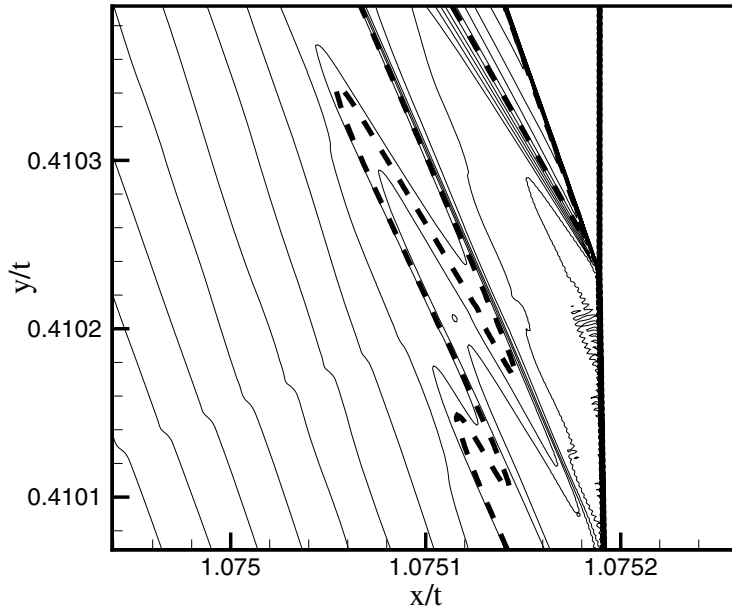
(b) Pressure

FIG. 6. Contour plots over the full numerical domain, showing what appears to be a Mach reflection—three shocks and a contact discontinuity (visible as a jump in the Mach contours in (a)) meeting in a point. The Mach contour spacing in (a) and the pressure contour spacing in (b) are both 0.002. The full grid contains 2250×2710 finite volume cells.

the Mach number is 0. As the shock moves it induces a flow in the fluid behind it and a corresponding increase in pressure. The reflected shock is much weaker than the incident shock and decreases in strength as it moves away from the apparent triple point. The Mach shock increases in strength as it moves away from the triple point, reaching a maximum at the wall where it becomes a normal shock. Here, the pressure and the induced flow velocity are largest. A very weak contact discontinuity can be seen in the Mach contours in Figure 6(a). This is not visible in the plot in (b) because pressure does not jump across a contact discontinuity.



(a)



(b)

FIG. 7. The solution near the triple point for $M = 1.075$ and $\theta = 15$ degrees. The Mach contour spacing is 0.001 in (a) and 0.0005 in (b). The dashed line in both plots is the sonic line. The refined uniform grid is contained within the box shown in (a) and has 300×1000 cells ($\Delta\xi = \Delta\eta = 1 \times 10^{-6}$). Two reflected shock/expansion wave pairs are clearly visible, with indications of a third. A contact discontinuity appears as a very weak jump in Mach number.

In Figure 7(a), we show Mach number contours in the most refined region near the apparent triple point. The refined uniform grid, as indicated, is approximately aligned with the reflected shock. The dashed line in the figure is the numerically

TABLE 4.2

Approximate values of the reflected shock strengths for the three reflected shocks visible in Figure 7, beginning with the leading reflected shock, from the numerical data. For each shock, ρ_1 and ρ_0 denote the approximate values of ρ ahead of and behind the shock, respectively.

Shock	ρ_1	ρ_0	$[\rho]$
1	1.577	1.596	0.019
2	1.592	1.596	0.004
3	1.594	1.596	0.002

computed location of the sonic line, (3.4). (This sonic line is displayed more clearly in Figure 8(a).) Flow to the right of this line is supersonic, and the figure shows that the solution contains a small region of supersonic flow behind the triple point. There is an expansion fan centered at the leading triple point, but it cannot be seen clearly at this level of magnification. To show this expansion fan more clearly, in Figure 7(b) we show an enlargement of the solution, using more closely spaced contours, in a tiny region near the confluence of the incident, reflected, and Mach shocks. Behind the leading triple point, there is a sequence of very weak shocks that intersect the Mach shock, forming a sequence of triple points, with a very weak expansion fan centered at each triple point. Each shock-expansion wave pair in the sequence is smaller and weaker than the one preceding it. Three reflected shocks appear to be visible in the plots in Figure 7(a)–(b). Their approximate strengths, beginning with the leading reflected shock, are given in Table 4.2. The jump $[\rho]$ in ρ across a reflected shock is measured near the point where the flow behind the shock is sonic. This point is very close to the corresponding triple point on the Mach shock, as shown in Figure 7. In principle, a contact discontinuity originates at each triple point. However, the only contact discontinuity that is strong enough to be resolved numerically is the one at the leading triple point.

To depict the regions of supersonic and subsonic flow in a Guderley Mach reflection, we plot widely spaced Mach contours and the sonic line near the triple point in Figure 8(a). In the plot in (b), we give a cross section of Mach number \bar{M} taken vertically through the region shown in the plot in (a), at a location slightly to the left of the Mach shock. The height $\Delta(y/t)$ of the supersonic region behind the triple point is approximately 0.00075, and the width $\Delta(x/t)$ is approximately 0.0001. Here, the height $\Delta(y/t)$ is a numerical estimate of the difference between the maximum value of y/t on the sonic line and the minimum value of y/t at the rear sonic point on the Mach shock. The width $\Delta(x/t)$ is an estimate of the width of the supersonic region at the value of y/t corresponding to the leading triple point. The height of the supersonic region is approximately 0.6% of the length of the Mach shock.

We found that a certain minimum grid resolution was necessary to resolve the supersonic region behind the triple point. As we refined the grid beyond this minimum resolution, a detailed flowfield structure became visible in the supersonic region. Figure 9 shows Mach number contours for a sequence of solutions computed on successively refined grids. In Figure 9(a)–(b), the sonic line appears fairly smooth. The supersonic patch appears to be shock-free. After two further grid refinements, each by a factor of two in both x/t and y/t (Figure 9(c)), a shock is visible behind the leading triple point. Our finest grid solution is shown in the plot in Figure 9(d). Two shocks are visible behind the leading triple point. Further refinement of the grid resulted in almost no observable change in the solution, as shown in the plot in Figure 10, an indication of grid convergence. At resolutions lower than the one shown in Figure 9(a), the supersonic region disappears entirely, and the sonic line runs down the inside of

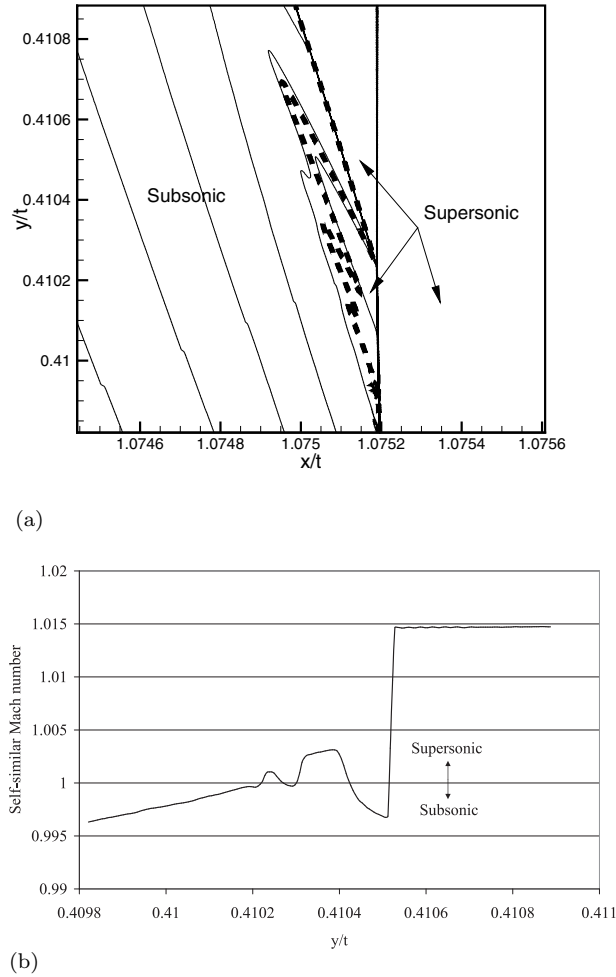


FIG. 8. The supersonic and subsonic regions near the triple point. The dashed line in (a) is the sonic line. It delineates the supersonic patch within the subsonic zone behind the triple point; the Mach contour spacing is 0.0025. In (b) a vertical cross section of \bar{M} is taken at the location $x/t = 1.0751$, slightly to the left of the incident shock/Mach stem. The large jump is the leading reflected shock. Note the crossings at $\bar{M} = 1$, indicating jumps across weak reflected shocks or smooth transitions across the sonic line.

the reflected shock, through the triple point, and down the Mach shock.

Figure 11 illustrates the size and location of the region where extreme local grid refinement is performed. The refined grid area is too small to be visible in the main plot shown in Figure 11. The inset figures show enlargements of the solution contained within the small rectangular box centered about the apparent triple point, as indicated. The solution shown in the smaller inset figure also contains a small box centered at the apparent triple point, indicating the approximate size and location of the region shown in Figures 7(a) and 8(a).

To further explore the wedge angle–shock strength parameter range in which the triple point paradox occurs, we also computed a solution of the shock reflection

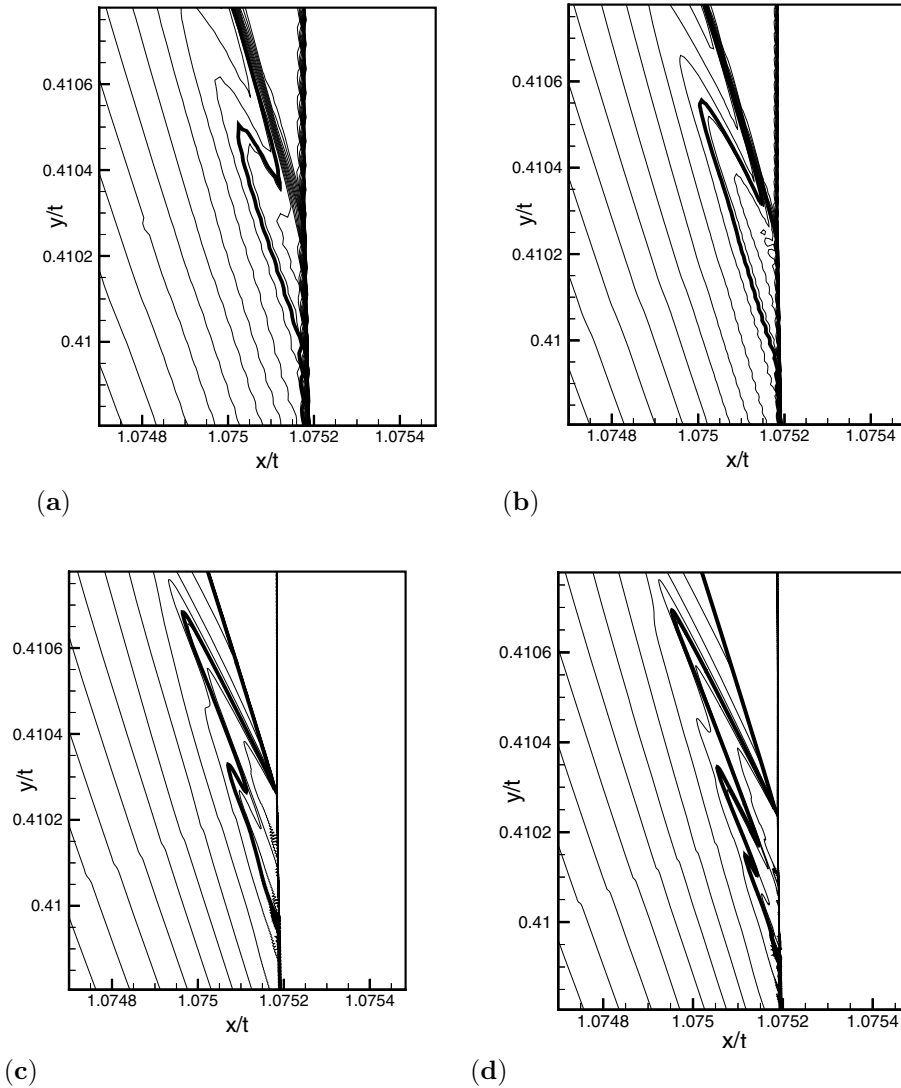


FIG. 9. A sequence of contour plots illustrating the effect of increasing grid resolution on the numerical solution. The figures show Mach contours in the refined grid area near the triple point, with a Mach contour spacing of 0.001. The heavy line is the sonic line. The mesh size used in the refined uniform grid area is $\Delta\xi = \Delta\eta = 1.6 \times 10^{-5}$ in (a), $\Delta\xi = \Delta\eta = 8 \times 10^{-6}$ in (b), $\Delta\xi = \Delta\eta = 2 \times 10^{-6}$ in (c), and $\Delta\xi = \Delta\eta = 1 \times 10^{-6}$ in (d). The area of the refined uniform grid in (c) and (d) is depicted in Figure 7(a); the refined uniform grids in (a) and (b) are slightly larger than the region shown. In (a), the refined uniform grid contains 64×64 grid cells. A supersonic region is visible as a bump in the sonic line, but it is poorly resolved. In (b), the refined uniform grid contains 128×128 grid cells. The supersonic region appears to be smooth. In (c), the refined uniform grid area contains 150×500 grid cells. There is a shock wave behind the leading triple point. In (d), the refined uniform grid area contains 300×1000 grid cells. Two shock waves are visible behind the leading triple point. The result of further refinement of the grid in (d) is shown in Figure 10.

problem with M equal to 1.04, wedge angle θ equal to 11.5 degrees, and ratio of specific heats γ equal to $5/3$. This choice of γ corresponds to shock reflection in a

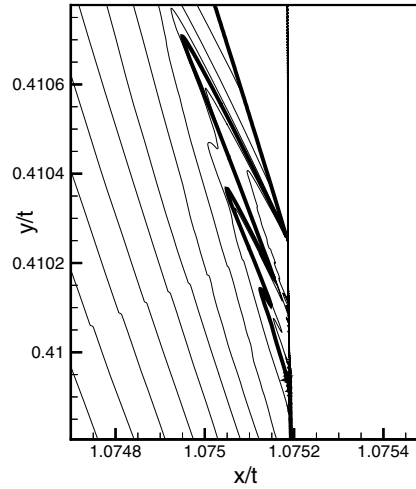


FIG. 10. Additional refinement of the grid used to obtain the solution in Figures 7, 8, and 9(d) by a factor of two in both x/t and y/t ($\Delta\xi = \Delta\eta = 5 \times 10^{-7}$) results in little change in the solution near the triple point. The Mach contours are plotted at the same levels of Mach number as the plots in Figure 9, and the size of the region shown is the same. The heavy line is the sonic line.

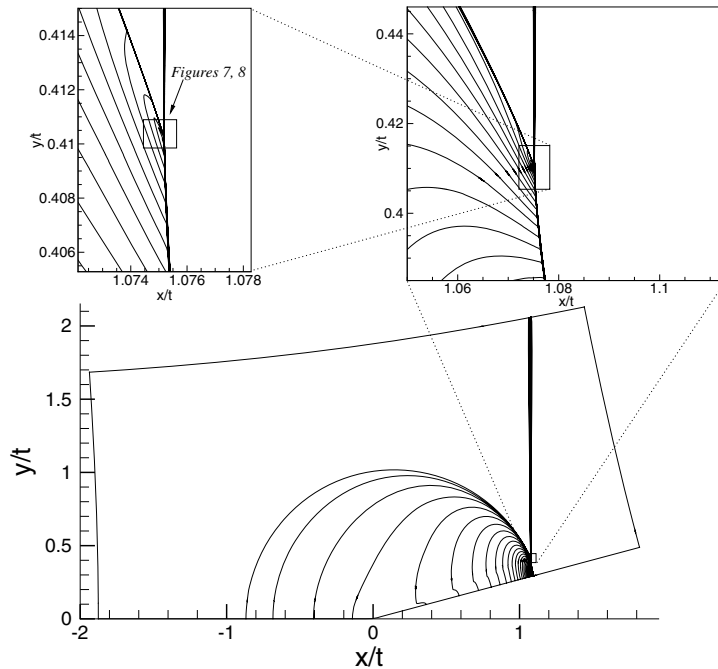


FIG. 11. An illustration of the approximate size and location of the region shown in the plots in Figures 7(a) and 8(a), which is contained in the small rectangular box shown in the smallest inset figure. The plot shows contour lines of ρ (density).

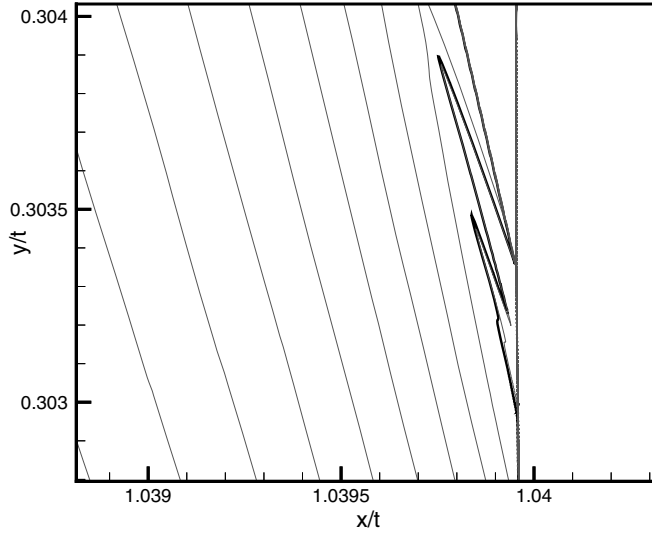


FIG. 12. A contour plot of Mach number near the apparent triple point for $M = 1.04$, $\theta = 11.5$ degrees, and $\gamma = 5/3$. The heavy line is the sonic line. The number of grid points in the full grid is approximately 11 million, of which $800 \times 2000 = 1.6$ million ($\Delta\xi = \Delta\eta = 5 \times 10^{-7}$) are devoted to the local refinement. The refined uniform grid is contained in the region shown in the plot.

monatomic gas ($\gamma = 1.4$ corresponds to a diatomic gas such as air). These data again correspond to parameter $a \approx 1/2$ in the UTSDE model used in [16]. Figure 12 shows Mach number contours and the sonic line in the neighborhood of the apparent triple point. Just as in our solution for $M = 1.075$, $\theta = 15$ degrees, and $\gamma = 1.4$, there is a sequence of triple points, reflected shocks, and expansion fans behind the leading triple point. Two reflected shock/expansion wave pairs are evident from the shape of the sonic line, with a slight indication of a third. At this lower shock strength, twice the grid refinement in both directions was required to obtain a solution comparable to that obtained for a $M = 1.075$ incident shock. The incident, reflected, and Mach shocks at the leading triple point are so weak that no contact discontinuity is visible.

5. Discussion. These numerical results display a structure that is remarkably similar to the solutions of the shock reflection problem for the UTSDE model in [16] (compare Figures 7(a) and (b) with Figures 5 and 6 of [16], for example) and to its analogue for the nonlinear wave system in [17] (see Figure 6, p. 331). In all three cases, a weak shock reflection in a parameter range where regular reflection is impossible results in a sequence of triple points and supersonic patches in a tiny region behind the leading triple point, with an expansion fan originating at each triple point. The results presented here appear to confirm the validity of the UTSDE as a model for weak shock reflection. In addition, it now appears that this solution structure may occur generically in a class of conservation laws that includes the physically important Euler equations of gasdynamics.

An important feature of the numerical solution is the small size of the supersonic region. In our solution for a shock with $M = 1.075$ impinging on a 15 degree ramp, the height of the supersonic region is approximately 0.6% of the length of the Mach shock. This can be compared to the results in [16]. The UTSDE model used there depends on a single order-one transonic similarity parameter $a = \theta/\sqrt{2(M^2 - 1)}$. Solutions were

obtained over a range of values of a , and the supersonic regions found in the solutions varied in height from approximately 0.05% to 3% of the length of the Mach shock, depending on the value of a . Our $M = 1.075/15^\circ$ problem corresponds to $a = 0.5$, a value for which the height of the supersonic region in [16] was approximately 1.9% of the height of the Mach shock, somewhat larger than the region obtained in the present work. The UTSDE are an asymptotic reduction of the Euler equations in the limit of weak shocks and thin wedges (see [8]), and we do not expect exact agreement between solutions of the problem for the asymptotic equations and the problem for the Euler equations. For wedge angles closer to 0 and Mach numbers closer to 1, we would expect closer agreement with the solutions in [16]. The computation we performed with $M = 1.04$, $\theta = 11.5$ degrees displayed in Figure 12 serves as a check of this statement. The height of the supersonic region in our solution for this choice of parameters is approximately 1% of the length of the Mach shock, indeed closer to the figure of 1.9% obtained in [16].

The supersonic regions behind the triple point in our solutions for $M = 1.075$, $\theta = 15^\circ$ and $M = 1.04$, $\theta = 11.5^\circ$ are much larger in height than in width. Defining an aspect ratio $\Delta(y/t)/\Delta(x/t)$, these solutions have aspect ratios of approximately 8:1 and 9:1, respectively. This quantity agrees closely with the solutions in [16]. There, solutions obtained over a range of values of a contain supersonic regions with aspect ratios from approximately 2.75:1 to 8.5:1. The solution in [16] with $a = 1/2$ has an aspect ratio of 8:1, approximately the same as the solutions presented here, which correspond to this value of a . Although the supersonic regions obtained in the present work are smaller in size than the one obtained in [16] for $a = 1/2$, the shape of the regions obtained agrees quite closely.

Table 4.2 gives an indication of how the reflected shock strength decays in the sequence of shocks/expansions which comprise a Guderley Mach reflection. From the table, the strength of the first three reflected shocks is approximately in the ratio 9.5 : 2 : 1. This is quite similar to the UTSDE result for $a = 1/2$ in [16]. There, four reflected shocks were visible in the solution; the strengths of the first three were in the approximate ratio 8 : 2 : 1. For the nonlinear wave system solution in [17], the ratio was approximately 12 : 3 : 1. We do not know precisely how the sequence of supersonic patches and shocks/expansions in Guderley Mach reflection decreases in size and strength, respectively, nor do we know if the sequence is finite or infinite.

The experimental results of Skews and Ashworth in [12] appear to confirm the existence of the Guderley Mach reflection structure reported here. The experiments were carried out on a 15° ramp with incident shock Mach numbers ranging from 1.05 to 1.1. The size of the expansion wave and terminating shocklet which were observed behind the leading triple point in experiments with measured Mach numbers of $M = 1.069$ and $M = 1.084$ was estimated to be less than 2% of the length of the Mach stem, a figure which, again, is somewhat larger than the wave structure observed numerically in the present work. The incident shock wave that is generated by the shock tube apparatus used in [12] is only approximately planar, however, and this may be one reason for the discrepancy. In addition, density gradients, which are visualized by the schlieren photo-optical technique used in [12], persist well beyond the supersonic patch into the subsonic region, making it difficult to estimate the extent of the supersonic patch from schlieren photographs. Nevertheless, the structure found in the experiments is very similar to the numerically computed Guderley Mach reflection solution. More recent experimental results [13] show more convincing evidence: the expansion fan and first terminating shocklet observed under conditions corresponding to $a \approx 1/2$ are more clearly visible, and the region appears to have an aspect ratio

similar to the value of approximately 8:1 obtained in the solutions presented here.

Guderley's resolution was largely correct: a fourth wave, a centered expansion fan, originates at the triple point, although Guderley did not have any evidence that this is what actually occurs, nor did he suggest that there might be, in fact, a sequence of expansion fans and triple points. It is interesting, as noted in [12], that experimental observations of weak shock reflections off thin wedges show that not only does an apparent Mach reflection occur but that the slip line disappears or becomes ill defined. Figures 6(a) and 7(a) show that the slip line still exists in a weak shock reflection, but that it is extremely weak, making it difficult to observe experimentally.

6. Conclusion. We have presented numerical evidence of a sequence of triple points, each containing a centered expansion fan, in solutions of a shock reflection problem for the full Euler equations. This result is in agreement with previous numerical solutions of shock reflection problems for the UTSDE and the nonlinear wave system. The present work provides further evidence that the reflection pattern we call Guderley Mach reflection occurs when a weak shock reflects off a thin wedge.

REFERENCES

- [1] W. BLEAKNEY AND A. H. TAUB, *Interaction of shock waves*, Rev. Modern Phys., 21 (1949), pp. 584–605.
- [2] M. BRIO AND J. K. HUNTER, *Mach reflection for the two-dimensional Burgers equation*, Phys. D, 60 (1992), pp. 194–207.
- [3] S. ČANIĆ AND B. L. KEYFITZ, *Quasi-one-dimensional Riemann problems and their role in self-similar two-dimensional problems*, Arch. Rational Mech. Anal., 144 (1998), pp. 233–258.
- [4] P. COLELLA AND L. F. HENDERSON, *The von Neumann paradox for the diffraction of weak shock waves*, J. Fluid Mech., 213 (1990), pp. 71–94.
- [5] K. G. GUDERLEY, *Considerations of the Structure of Mixed Subsonic-Supersonic Flow Patterns*, Air Material Command Tech. Report F-TR-2168-ND, ATI 22780, GS-AAF-Wright Field 39, U.S. Wright-Patterson Air Force Base, Dayton, OH, 1947.
- [6] L. F. HENDERSON, *On a class of multi-shock intersections in a perfect gas*, Aero. Q., 17 (1966), pp. 1–20.
- [7] L. F. HENDERSON, *Regions and boundaries for diffracting shock wave systems*, Z. Angew. Math. Mech., 67 (1987), pp. 73–86.
- [8] J. K. HUNTER AND M. BRIO, *Weak shock reflection*, J. Fluid Mech., 410 (2000), pp. 235–261.
- [9] J. K. HUNTER AND A. M. TEDDALL, *Weak shock reflection*, in A Celebration of Mathematical Modeling, D. Givoli, M. Grote, and G. Papanicolaou, eds., Kluwer Academic Press, New York, 2004, pp. 93–112.
- [10] J. VON NEUMANN, *Collected Works*, Vol. 6, Pergamon Press, New York, 1963.
- [11] A. SASOH, K. TAKAYAMA, AND T. SAITO, *A weak shock wave reflection over wedges*, Shock Waves, 2 (1992), pp. 277–281.
- [12] B. SKEWS AND J. ASHWORTH, *The physical nature of weak shock wave reflection*, J. Fluid Mech., 542 (2005), pp. 105–114.
- [13] B. SKEWS, *private communication*.
- [14] J. STERNBERG, *Triple-shock-wave intersections*, Phys. Fluids, 2 (1959), pp. 179–206.
- [15] E. G. TABAK AND R. R. ROSALES, *Focusing of weak shock waves and the von Neumann paradox of oblique shock reflection*, Phys. Fluids, 6 (1994), pp. 1874–1892.
- [16] A. M. TEDDALL AND J. K. HUNTER, *Self-similar solutions for weak shock reflection*, SIAM J. Appl. Math., 63 (2002), pp. 42–61.
- [17] A. M. TEDDALL, R. SANDERS, AND B. L. KEYFITZ, *The triple point paradox for the nonlinear wave system*, SIAM J. Appl. Math., 67 (2006), pp. 321–336.
- [18] E. VASIL'EV AND A. KRAIKO, *Numerical simulation of weak shock diffraction over a wedge under the von Neumann paradox conditions*, Comput. Math. Math. Phys., 39 (1999), pp. 1335–1345.
- [19] A. ZAKHARIAN, M. BRIO, J. K. HUNTER, AND G. WEBB, *The von Neumann paradox in weak shock reflection*, J. Fluid Mech., 422 (2000), pp. 193–205.